

## Coupling of CpCr(CO)<sub>3</sub> and Heterocyclic Dithiadiazolyl Radicals. Synthetic, X-ray Diffraction, Dynamic NMR, EPR, CV, and DFT Studies

Hui Fung Lau,<sup>†</sup> Pearly Chwee Ying Ang,<sup>†</sup> Victor Wee Lin Ng,<sup>†</sup> Seah Ling Kuan,<sup>†</sup> Lai Yoong Goh,<sup>\*,†</sup> Alexey S. Borisov,<sup>‡</sup> Paul Hazendonk,<sup>‡</sup> Tracey L. Roemmele,<sup>‡</sup> René T. Boéré,<sup>\*,‡</sup> and Richard D. Webster<sup>§</sup>

Department of Chemistry, National University of Singapore, Kent Ridge, Singapore 119260, Department of Chemistry and Biochemistry, University of Lethbridge, Lethbridge, Alberta, Canada T1K 3M4, and Division of Chemistry and Biological Chemistry, School of Physical & Mathematical Sciences, Nanyang Technological University, Singapore 637371

Received October 28, 2007

The reaction of the 1,2,3,5-dithiadiazolyls (4-R-C<sub>6</sub>H<sub>4</sub>CN<sub>2</sub>S<sub>2</sub>)<sub>2</sub> (R = Me, **2a**; Cl, **2b**; OMe, **2c**; and CF<sub>3</sub>, **2d**) and (3-NC-5-<sup>t</sup>Bu-C<sub>6</sub>H<sub>3</sub>CN<sub>2</sub>S<sub>2</sub>)<sub>2</sub> (**2e**) with [CpCr(CO)<sub>3</sub>]<sub>2</sub> (Cp = η<sup>5</sup>-C<sub>5</sub>H<sub>5</sub>) (**1**) at ambient temperature respectively yielded the complexes CpCr(CO)<sub>2</sub>(η<sup>2</sup>-S<sub>2</sub>N<sub>2</sub>CC<sub>6</sub>H<sub>4</sub>R) (R = 4-Me, **3a**; 4-Cl, **3b**; 4-OMe, **3c**; and 4-CF<sub>3</sub>, **3d**) and CpCr(CO)<sub>2</sub>(η<sup>2</sup>-S<sub>2</sub>N<sub>2</sub>CC<sub>6</sub>H<sub>3</sub>-3-(CN)-5-(<sup>t</sup>Bu)) (**3e**) in 35–72% yields. The complexes **3c** and **3d** were also synthesized via a salt metathesis method from the reaction of NaCpCr(CO)<sub>3</sub> (**1B**) and the 1,2,3,5-dithiadiazolium chlorides 4-R-C<sub>6</sub>H<sub>4</sub>-CN<sub>2</sub>S<sub>2</sub>Cl (R = OMe, **8c**; CF<sub>3</sub>, **8d**) with much lower yields of 6 and 20%, respectively. The complexes were characterized spectroscopically and also by single-crystal X-ray diffraction analysis. Cyclic voltammetry experiments were conducted on **3a–e**, EPR spectra were obtained of one-electron-reduced forms of **3a–e**, and variable temperature <sup>1</sup>H NMR studies were carried out on complex **3d**. Hybrid DFT calculations were performed on the model system [CpCr(CO)<sub>2</sub>S<sub>2</sub>N<sub>2</sub>CH] and comparisons are made with the reported CpCr(CO)<sub>2</sub>(π-allyl) complexes.

### 1. Introduction

In the context of our interest in the chemistry of [CpCr(CO)<sub>3</sub>]<sub>2</sub> (**1**) with S- and/or P-containing compounds, we have studied **1**-initiated interchalcogen cleavage in a variety of systems, viz. in homopolynuclear inorganic compounds,<sup>1</sup> in organic substrates, e.g., diphenyldichalcogenides Ph<sub>2</sub>E<sub>2</sub> (E = S, Se, Te),<sup>2</sup> bis(thiophosphoro)disulfanes, (R<sub>2</sub>P(S)S-)<sub>2</sub> (R = Ph<sup>3</sup> and <sup>i</sup>PrO,<sup>4</sup> respectively), tetraalkylthiuram disulfanes (R<sub>2</sub>NC(S)S-)<sub>2</sub>,<sup>5</sup> dibenzothiazolyl disulfane, (-SCSN(C<sub>6</sub>H<sub>4</sub>))<sub>2</sub>,<sup>6</sup>

and dithiobis(tetrazole) (PhN<sub>4</sub>CS)<sub>2</sub>.<sup>7</sup> For chalcogen–pnictogen bond cleavage, our previous work had dealt with the closo polyhedra P<sub>4</sub>E<sub>3</sub> (E = S,<sup>8</sup> Se<sup>9</sup>), the polymeric Sb<sub>2</sub>S<sub>3</sub>,<sup>10</sup> and Lawesson's reagent.<sup>11</sup> The richness of this chemistry is further extended by the homolytic cleavage of Cr–E bonds (E = N, P, S, Se) in CpCr complexes.<sup>12</sup>

\* Corresponding authors. L.Y.G.: present address, Division of Chemistry and Biological Chemistry, School of Physical and Mathematical Sciences, Nanyang Technological University, Singapore 637371; fax, +65 6316 6984; e-mail, LaiYoongGoh@ntu.edu.sg. R.T.B.: fax, +1-403-329-2057; e-mail: boere@uleth.ca.

<sup>†</sup> National University of Singapore.

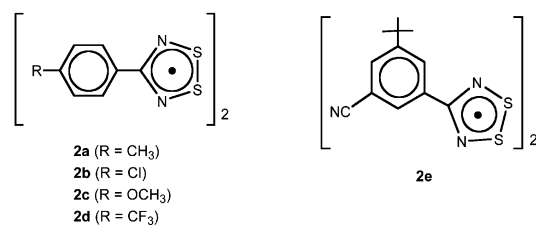
<sup>‡</sup> University of Lethbridge.

<sup>§</sup> Nanyang Technological University.

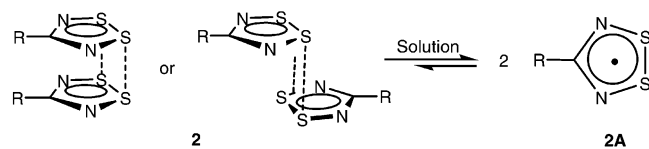
- (1) Goh, L. Y. *Coord. Chem. Rev.* **1999**, *185–186*, 257–276 and references therein.
- (2) (a) Goh, L. Y.; Tay, M. S.; Mak, T. C. W.; Wang, R.-J. *Organometallics* **1992**, *11*, 1711–1717. (b) Goh, L. Y.; Tay, M. S.; Lim, Y. Y.; Mak, T. C. W.; Zhou, Z.-Y. *J. Chem. Soc., Dalton Trans.* **1992**, 1239–1242. (c) Goh, L. Y.; Tay, M. S.; Chen, W. *Organometallics* **1994**, *13*, 1813–1820.
- (3) Goh, L. Y.; Leong, W. K.; Leung, P.-H.; Weng, Z.; Haiduc, I. J. *Organomet. Chem.* **2000**, *607*, 64–71.

- (4) Goh, L. Y.; Weng, Z.; Leong, W. K.; Haiduc, I.; Lo, K. M.; Wong, R. C. S. *J. Organomet. Chem.* **2001**, *631*, 67–75.
- (5) (a) Goh, L. Y.; Weng, Z.; Leong, W. K.; Leung, P. H. *Angew. Chem., Int. Ed.* **2001**, *40*, 3236–3239. (b) Goh, L. Y.; Weng, Z.; Leong, W. K.; Leung, P. H. *Organometallics* **2002**, *21*, 4398–4407. (c) Goh, L. Y.; Weng, Z.; Hor, T. S. A.; Leong, W. K. *Organometallics* **2002**, *21*, 4408–4414.
- (6) Goh, L. Y.; Weng, Z.; Leong, W. K.; Vittal, J. J. *J. Am. Chem. Soc.* **2002**, *124*, 8804–8805.
- (7) Ng, V. W. L.; Weng, Z.; Vittal, J. J.; Koh, L. L.; Tan, G. K.; Goh, L. Y. *J. Organomet. Chem.* **2005**, *690*, 1157–1165.
- (8) (a) Goh, L. Y.; Chen, W.; Wong, R. C. S. *Angew. Chem., Int. Ed. Engl.* **1993**, *32*, 1728–1729. (b) Goh, L. Y.; Chen, W.; Wong, R. C. S.; Karaghiosoff, K. *Organometallics* **1995**, *14*, 3886–3896.
- (9) Goh, L. Y.; Chen, W.; Wong, R. C. S. *Organometallics* **1999**, *18*, 306–314.
- (10) Goh, L. Y.; Chen, W.; Wong, R. C. S. *Chem. Commun.* **1999**, 1481–1482.
- (11) (a) Weng, Z.; Leong, W. K.; Vittal, J. J.; Goh, L. Y. *Organometallics* **2003**, *22*, 1645–1656. (b) Weng, Z.; Leong, W. K.; Vittal, J. J.; Goh, L. Y. *Organometallics* **2003**, *22*, 1657–1662.

Chart 1



Scheme 1



In this present study, we have initiated an investigation of the reaction of **1** with several substituted aryl 1,2,3,5-dithiadiazolyls, viz. (4-R-C<sub>6</sub>H<sub>4</sub>CN<sub>2</sub>S<sub>2</sub>)<sub>2</sub> (R = Me, **2a**; Cl, **2b**; OMe, **2c**; CF<sub>3</sub>, **2d**; R<sup>1</sup> = 3-CN, R<sup>2</sup> = 5-<sup>t</sup>Bu, **2e**), shown in Chart 1. The dithiadiazolyls exist in monomer–dimer equilibrium in solution (Scheme 1).<sup>13,14</sup> This class of free radicals has attracted special attention in the last few decades,<sup>15</sup> on account of their utility as building blocks for molecular electronic<sup>16</sup> and magnetic materials<sup>15d,g</sup> and as chelating ligands for low oxidation state metal complexes, especially where the ligand remains spin-bearing.<sup>17–26</sup> In the present context, their five-membered heterocyclic rings

present possibilities of C–N, N–S, and S–S cleavage reactivity, all characteristic of the monomeric radical derivative of **1**.<sup>27,12</sup> In a recent communication<sup>28a</sup> and several conference proceedings,<sup>28b,c</sup> we have reported completely unprecedented  $\pi$ -complexes of these main-group radicals with **1A**. Here we provide full experimental details for these novel results and report on their electronic, dynamic NMR, and electrochemical properties, including in situ EPR spectroelectrochemical studies that identify their radical anions.

By virtue of the availability of 7 $\pi$ -electrons in the ring and a plethora of in-plane electron lone pairs, metal complexes of dithiadiazolyls exhibit variable coordination and ligand–metal bonding.<sup>24,26</sup> An oxidative addition occurs with zerovalent Pd and Pt phosphine complexes, resulting in S–S bond cleavage and chelation of the resulting disulfide to the metal. With Fe<sub>2</sub>(CO)<sub>9</sub> or Fe<sub>3</sub>(CO)<sub>12</sub>,<sup>17,18</sup> [CpNi(CO)]<sub>2</sub>,<sup>19</sup> and [Pd(dppe)]<sub>2</sub>,<sup>22</sup> the ring-opened heterocyclic ligand bridges two metal centers in  $\mu_2$ - $\eta^2, \eta^2$  mode, as shown in **A–D** in Chart 2; within **B** and **C** there is a retention of paramagnetism, while in **A** and **D** formal hydrogen abstraction by a ligand nitrogen atom occurs to quench paramagnetism. The utilization of two functional ligands leads to trimetallic complexes, **E**. Cooperative binding with N-donor ligands like  $\alpha$ -pyridyl, **F**,<sup>29</sup> or pyrazine, **G**,<sup>30</sup> leads to N,N'-chelated complexes that retain the CN<sub>2</sub>S<sub>2</sub> unpaired electron.

The formal analogy between thiazyl ring compounds and aromatic or antiaromatic hydrocarbons has been useful for understanding the diverse chemistry of this class of compounds.<sup>15</sup> In that context, the *absence* of  $\pi$ -complexes to transition metals is particularly noteworthy. A theoretical treatment of  $\eta^4$ -S<sub>2</sub>N<sub>2</sub> coordination was put forward many

- (12) Weng, Z.; Goh, L. Y. *Acc. Chem. Res.* **2004**, *37*, 187–199 and references therein.
- (13) (a) Brooks, W. V. F.; Burford, N.; Passmore, J.; Schriver, M. J.; Sutcliffe, L. H. *J. Chem. Soc., Chem. Commun.* **1987**, 69–71. (b) Fairhurst, S. A.; Johnson, K. M.; Sutcliffe, L. H.; Preston, K. F.; Banister, A. J.; Hauptman, Z. V.; Passmore, J. *J. Chem. Soc., Dalton Trans.* **1986**, 1465–1472.
- (14) (a) Aherne, C.; Banister, A. J.; Luke, A. W.; Rawson, J. M.; Whitehead, R. J. *J. Chem. Soc., Dalton Trans.* **1992**, 1277–1282. (b) Banister, A. J.; Lavender, I.; Rawson, J. M.; Clegg, W.; Tanner, B. K.; Whitehead, R. J. *J. Chem. Soc., Dalton Trans.* **1993**, 1421–1429. (c) Banister, A. J.; Batsanov, A. S.; Dawe, O. G.; Herbertson, P. L.; Howard, J. A. K.; Lynn, S.; May, I.; Smith, J. N. B.; Rawson, J. M.; Rogers, T. E.; Tanner, B. K.; Antorrena, G.; Palacio, F. *J. Chem. Soc., Dalton Trans.* **1997**, 2539–2542.
- (15) See the following articles/reviews and references therein: (a) Banister, A. J.; Rawson, J. M. *Chem. Br.* **1992**, 148–152. (b) Cordes, A. W.; Haddon, R. C.; Oakley, R. T. In *Studies in Inorganic Chemistry, Vol. 14: The Chemistry of Inorganic Ring Systems*; Stuedel, R., Ed.; Elsevier, Amsterdam, 1992; Chapter 16, pp 295–348. (c) Rawson, J. M.; Banister, A. J.; Lavender, I. *Adv. Heterocycl. Chem.* **1995**, *62*, 137–247. (d) Rawson, J. M.; Palacio, F. *Struct. Bonding* **2001**, *100*, 93–128. (e) Alberola, A.; Less, R. J.; Pask, C. M.; Rawson, J. M.; Palacio, F.; Oliete, P.; Paulsen, C.; Yamaguchi, A.; Farley, R. D.; Murphy, D. M. *Angew. Chem., Int. Ed.* **2003**, *42*, 4782–4785. (f) Boeré, R. T.; Mook, K. H. *Phosphorus, Sulfur, and Silicon* **1994**, *93–94*, 451–452. (g) Rawson, J. M.; Alberola, A.; Whalley, A. J. *Mat. Chem.* **2006**, *16*, 2560–2575.
- (16) Cordes, A. W.; Haddon, R. C.; Oakley, R. T. *Adv. Mater.* **1994**, *6*, 798–802.
- (17) (a) Boeré, R. T.; Mook, K. H.; Klassen, V.; Weaver, J.; Lentz, D.; Michael-Schulz, H. *Can. J. Chem.* **1995**, *73*, 1444–1453. (b) Klassen, V.; Preuss, K.; Mook, K. H.; Boeré, R. T. *Phosphorus, Sulfur Silicon* **1994**, *93–94*, 449–450.
- (18) Banister, A. J.; Gorrell, I. B.; Clegg, W.; Jørgensen, K. A. *J. Chem. Soc., Dalton Trans.* **1989**, 2229–2233.
- (19) Banister, A. J.; Gorrell, I. B.; Clegg, W.; Jørgensen, K. A. *J. Chem. Soc., Dalton Trans.* **1991**, 1105–1109.
- (20) Banister, A. J.; Gorrell, I. B.; Lawrence, S. E.; Lehmann, C. W.; May, I.; Tate, G.; Blake, A. J.; Rawson, J. M. *J. Chem. Soc., Chem. Commun.* **1994**, 1779–1780.
- (21) Banister, A. J.; May, I. *Phosphorus, Sulfur Silicon* **1994**, *93–94*, 447–448.

- (22) Banister, A. J.; Howard, J. A. K.; May, I.; Rawson, J. M. *J. Chem. Soc., Chem. Commun.* **1997**, 1763–1764.
- (23) Banister, A. J.; Gorrell, I. B.; Howard, J. A. K.; Lawrence, S. E.; Lehman, C. W.; May, I.; Rawson, J. M.; Tanner, B. K.; Gregory, C. I.; Blake, A. J.; Fricker, S. P. *J. Chem. Soc., Dalton Trans.* **1997**, 377–384.
- (24) Banister, A. J.; May, I.; Rawson, J. M.; Smith, J. N. B. *J. Organomet. Chem.* **1998**, *550*, 241–253 (review) and references therein.
- (25) Wong, W.-K.; Sun, C.; Wong, W.-Y.; Kwong, D. W. J.; Wong, W. T. *Eur. J. Inorg. Chem.* **2000**, 1045–1054.
- (26) Preuss, K. E. *Dalton Trans.* **2007**, 2357–2369.
- (27) See for instance the following: (a) Adams, R. D.; Collins, D. E.; Cotton, F. A. *J. Am. Chem. Soc.* **1974**, *96*, 749–754. (b) Madach, T.; Vahrenkamp, H. *Z. Naturforsch. B* **1978**, *33b*, 1301–1303. (c) Goh, L. Y.; D'Aniello, M. J., Jr.; Slater, S.; Muettterties, E. L.; Tavanaiepour, I.; Chang, M. I.; Fredrich, M. F.; Daz, V. W. *Inorg. Chem.* **1979**, *18*, 192–197. (d) McLain, S. J. *J. Am. Chem. Soc.* **1988**, *110*, 643–644. (e) Baird, M. C. *Chem. Rev.* **1988**, *88*, 1217–1227. (f) Goh, L. Y.; Lim, Y. Y. *J. Organomet. Chem.* **1991**, *402*, 209–214.
- (28) (a) Lau, H. F.; Ng, V. W. L.; Koh, L. L.; Tan, G. K.; Goh, L. Y.; Roemmele, T. L.; Seagrave, S. D.; Boeré, R. T. *Angew. Chem., Int. Ed. Engl.* **2006**, *45*, 4498–4501. (b) Boeré, R. T.; Roemmele, T. L.; Seagrave, S. D.; Goh, L. Y. 88th Canadian Chemistry Conference and Exhibition, Saskatoon, Canada, May 28–June 1, 2005, Abstract #490. (c) Boeré, R. T.; Yu, X.; Goh, L.-Y.; Ng, V. W. L.; Ang, C. W. P.; Kuan, S. L.; Lau, H. F. 89th Canadian Chemistry Conference and Exhibition, Halifax, NS, Canada, May 27–31, 2006 (Abstract #0061).
- (29) (a) Hearn, N. G. R.; Preuss, K. E.; Richardson, J. F.; Bin-Salamon, S. *J. Am. Chem. Soc.* **2004**, *126*, 9942–9943. (b) Britten, J.; Hearn, N. G. R.; Preuss, K. E.; Richardson, J. F.; Bin-Salamon, S. *Inorg. Chem.* **2007**, *46*, 3934–3945.
- (30) (a) Jennings, M.; Preuss, K. E.; Wu, J. *Chem. Commun.* **2006**, 341. (b) Hearn, N. G. R.; Hesp, K. D.; Jennings, M.; Korcok, J. L.; Preuss, K. E.; Smithson, C. S. *Polyhedron* **2007**, *26*, 2047–2053.



NMR data could not be obtained on this product due to sample decomposition in solution.

**CpCr(CO)<sub>2</sub>(η<sup>2</sup>-S<sub>2</sub>N<sub>2</sub>CC<sub>6</sub>H<sub>4</sub>CF<sub>3</sub>) (3d).** A similar procedure using **2d** (100 mg, 0.20 mmol) and **1** (80 mg, 0.20 mmol) gave **3d** (ca. 62 mg, 0.15 mmol, 37% yield) together with **4** (ca. 36 mg, 0.10 mmol, 48% yield).

**Data for 3d.** Anal. Calcd for CpCr(CO)<sub>2</sub>(S<sub>2</sub>N<sub>2</sub>CC<sub>6</sub>H<sub>4</sub>CF<sub>3</sub>): C, 42.66; H, 2.15; N, 6.63; S, 15.18. Found: C, 42.70; H, 2.35; N, 6.49; S, 15.16. <sup>1</sup>H NMR: δ(Cp) 3.79 (s, 5H); δ(C<sub>6</sub>H<sub>4</sub>) 7.99 (br, ν<sub>1/2</sub> = ca. 14 Hz, 2H) and 7.26 (d, 2H). IR (KBr, cm<sup>-1</sup>): ν(C=O) 1975 vs and 1918 vs. FAB<sup>+</sup>-MS: *m/z* 422 [M + 1]<sup>+</sup>, 366 [M - 2CO]<sup>+</sup>, 195 [CpCrS<sub>2</sub>N]<sup>+</sup>. As for **3c**, <sup>13</sup>C NMR data were not obtained.

All the complexes (**3a–e**) were found to be air-stable in the solid state. <sup>1</sup>H NMR spectral scans of **3a–e** in benzene-*d*<sub>6</sub> showed that all the complexes almost totally converted to Cp<sub>4</sub>Cr<sub>4</sub>S<sub>4</sub> (**5**) (δ(Cp) 4.91<sup>35</sup>) after a day at ambient temperature. This instability contributed to our failure to obtain <sup>13</sup>C NMR data.

**2.3. Reactions of the Dithiadiazolium Chlorides (8c, 8d) and S<sub>8</sub> with Sodium Cyclopentadienylchromium Tricarbonyl Na-[CpCr(CO)<sub>3</sub>] (1B).** CpCr(CO)<sub>2</sub>(η<sup>2</sup>-S<sub>2</sub>N<sub>2</sub>CC<sub>6</sub>H<sub>4</sub>OMe) (**3c**). Na-[CpCr(CO)<sub>3</sub>] (**1B**) (20 mg, 0.09 mmol) and 4-Ome-C<sub>6</sub>H<sub>4</sub>CN<sub>2</sub>S<sub>2</sub>Cl (**8c**) (24 mg, 0.1 mmol) were dissolved in a precooled (-29 °C) solvent mixture of toluene/THF (1:1, 12 mL). The resultant dark red solution was immediately concentrated to ca. 2 mL, adsorbed onto Celite, and subsequently evacuated to dryness. A slurry of the Celite adsorbate in hexane-toluene (ca. 1 mL) was loaded onto a silica gel column (1 × 8 cm) prepared in *n*-hexane. Elution gave four fractions: (i) a green eluate in *n*-hexane/toluene (3:1, 25 mL), which on concentration gave deep green crystals of [CpCr(CO)<sub>2</sub>]<sub>2</sub>S (**4**) (ca. 9 mg, 0.02 mmol, 53% yield); (ii) a reddish brown eluate in *n*-hexane/toluene (1:2, 25 mL), which yielded yellow solid 3,7-(4-MeO-C<sub>6</sub>H<sub>4</sub>)<sub>2</sub>{CN<sub>2</sub>S<sub>2</sub>N<sub>2</sub>C} (**7c**) (ca. 7 mg, 0.02 mmol, 40%);<sup>36</sup> (iii) a red eluate in *n*-hexane/toluene (1:5, 30 mL), which yielded a fine red crystalline solid of CpCr(CO)<sub>2</sub>(η<sup>2</sup>-S<sub>2</sub>N<sub>2</sub>CC<sub>6</sub>H<sub>4</sub>-4-OMe) (**3c**), characterized as above (ca. 9 mg, 0.02 mmol, 26% crude yield) [Recrystallization of this in toluene/hexane gave after a day at -29 °C a mixture of red crystals of CpCr(CO)<sub>2</sub>(η<sup>2</sup>-S<sub>2</sub>N<sub>2</sub>CC<sub>6</sub>H<sub>4</sub>-4-OMe) (**3c**) (2 mg, 0.005 mmol, 6% yield) and unidentified fine yellow flakes (<1 mg), from which the red crystals could be physically separated with the aid of a microscope.]; and (iv) a brown eluate in THF, which yielded a 1:1:3 mixture (2 mg) of **4**, **5**, and μ<sup>2</sup>,η<sup>2</sup>-S<sub>2</sub>[CpCr(CO)<sub>2</sub>]<sub>2</sub> (**6**), the latter indicated by the presence of δ(Cp) 4.13 in the <sup>1</sup>H NMR spectrum. An immovable pale blue band (ca. 2 mm thick) was left uneluted on the column. During the process of column chromatography, some effervescence (probably of CO) was observed.

**Data for 7c.** IR (KBr, cm<sup>-1</sup>): 1604 m, 1506 m, 1468 w, 1440 w, 1382 s, 1301 w, 1252 s, 1225 m, 1168 m, 1113 w, 1030 m, 943 w, 840 w, 823 w, 790 w, 730 w, 651 m, 599 w, 524 w, 466 w. FAB<sup>+</sup>-MS: *m/z* 358 [M]<sup>+</sup>, 225 [N<sub>3</sub>S<sub>2</sub>CC<sub>6</sub>H<sub>4</sub>OCH<sub>3</sub>]<sup>+</sup>, 211 [N<sub>2</sub>S<sub>2</sub>-CC<sub>6</sub>H<sub>4</sub>OCH<sub>3</sub>]<sup>+</sup>, 179 [N<sub>2</sub>SCC<sub>6</sub>H<sub>4</sub>OCH<sub>3</sub>]<sup>+</sup>, 165 [NSCC<sub>6</sub>H<sub>4</sub>OCH<sub>3</sub>]<sup>+</sup>, 150 [NSCC<sub>6</sub>H<sub>4</sub>OCH<sub>3</sub>]<sup>+</sup>, 133 [NCC<sub>6</sub>H<sub>4</sub>OCH<sub>3</sub>]<sup>+</sup>, 103 [NCC<sub>6</sub>H<sub>4</sub>]<sup>+</sup>, in agreement with literature data.<sup>36</sup>

**CpCr(CO)<sub>2</sub>(η<sup>2</sup>-S<sub>2</sub>N<sub>2</sub>CC<sub>6</sub>H<sub>4</sub>CF<sub>3</sub>) (3d).** Likewise, the reaction of 4-CF<sub>3</sub>-C<sub>6</sub>H<sub>4</sub>CN<sub>2</sub>S<sub>2</sub>Cl (**8d**) (21 mg, 0.07 mmol) with **1B** (16 mg, 0.07 mmol) led to the isolation of **3d** (ca. 6 mg, 0.01 mmol, 20% yield), along with **4** (ca. 23 mg, 0.06 mmol, 24% yield) and small amounts of **5** and 3,7-(4-CF<sub>3</sub>-C<sub>6</sub>H<sub>4</sub>)<sub>2</sub>{CN<sub>2</sub>S<sub>2</sub>N<sub>2</sub>C} (**7d**) (ca. 1 mg,

0.002 mmol, 7%).<sup>34a</sup> **6** was not observed in this reaction, as with the earlier cases. Characterization of **3d** is as given in section 2.2 above.

**Data for 7d.** IR (KBr, cm<sup>-1</sup>): ν(C-H) 2928 w; ν(other bands) 1612 w, 1412 w, 1370 w, 1317 m, 1171 w, 1135 w, 1109 w, 1066 w, 1015 w, 944 w, 850 w, 685 w, 644 w, 590 w, 529 w, 449 w. EI-MS: *m/z* 434 [RCN<sub>2</sub>S<sub>2</sub>N<sub>2</sub>CR<sup>+</sup>, R = CF<sub>3</sub>C<sub>6</sub>H<sub>4</sub>], 263 [RCN<sub>3</sub>S<sub>2</sub><sup>+</sup>], 249 [RCN<sub>2</sub>S<sub>2</sub><sup>+</sup>], 203 [RCNS], 46 [SN<sup>+</sup>], in agreement with literature data.<sup>34a</sup>

It was found that, at ambient temperature, these reactions gave almost exclusively [CpCr(CO)<sub>2</sub>]<sub>2</sub>S, a precursor to Cp<sub>4</sub>Cr<sub>4</sub>S<sub>4</sub>, which is the thermodynamic sink for CpCr-thiolato type of complexes.<sup>1,12</sup>

**Reaction with S<sub>8</sub>.** A slurry of Na[CpCr(CO)<sub>3</sub>] (**1B**) (22 mg, 0.1 mmol) and S<sub>8</sub> (2.2 mg, ca. 0.01 mmol) in THF was stirred for 5 min and the resultant dark brown solution was subsequently evacuated to dryness. The residue was extracted with toluene (ca. 3 × 2 mL), leaving an insoluble dark yellow solid of unreacted **1B**, identified by its <sup>1</sup>H NMR spectrum [δ(Cp) 4.29 in acetone-*d*<sub>6</sub>].<sup>37</sup> The toluene extract was evacuated to dryness (ca. 2 mg) and its <sup>1</sup>H NMR spectra showed a 4:2 mixture of [CpCr(CO)<sub>2</sub>]<sub>2</sub>S (**4**) (7% yield) and μ<sup>2</sup>,η<sup>2</sup>-S<sub>2</sub>[CpCr(CO)<sub>2</sub>]<sub>2</sub> (**6**) (24%), identified by their Cp proton resonances.<sup>38</sup>

**2.4. Crystal Structure Analyses.** Diffraction-quality crystals were obtained from solutions in toluene as follows: **3a** as dark red needles after slow evaporation of a concentrated solution for 2 days at ambient temperature, and **3b** as dark red hexagons upon layering with ether after 2 days at -29 °C. **3c** and **3d** were obtained as dark red needles from solutions of toluene layered with hexane after 3 days at -29 °C, and **3e** was obtained as dark red needles upon layering with hexane after 2 days at -29 °C. Crystals of **2d** were grown by vacuum sublimation in a three-zone tube furnace as described previously.<sup>39</sup>

The crystals were mounted on quartz fibers. X-ray data were collected on a Bruker AXS SMART APEX CCD diffractometer (complexes **3a**, **3b**, **3e**, and **2d**) or a Siemens SMART diffractometer, equipped with a CCD detector (complexes **3c** and **3d**), using Mo Kα radiation (λ = 0.710 73 Å). The data were corrected for Lorentz and polarization effects with the SMART suite of programs<sup>40</sup> and for adsorption effects with SADABS.<sup>41</sup> Structure solution and refinement were carried out with the SHELXTL suite of programs.<sup>42</sup> The structure was solved by direct methods to locate the heavy atoms, followed by difference maps for the light, non-hydrogen atoms. The Cp, aryl, and alkyl hydrogen atoms were placed in calculated positions. In **3e**, the <sup>t</sup>Bu group was found to be disordered; a refinement model using two staggered groups was used for the structure, and the refined occupancies are 60/40. Data collection and processing parameters are given in Table 1. Atom numbering schemes are presented in Figure 2 for **3c,d**; those for **3a,b,e** are as in the preliminary communication.<sup>28a</sup>

**2.5. Electrochemistry and SEPR Spectroscopy.** Voltammetric experiments were conducted with a computer-controlled Eco

- (37) Behrens, U.; Edelmann, F. *J. Organomet. Chem.* **1984**, *263*, 179–182.  
 (38) (a) Greenhough, T. J.; Kolthammer, B. W. S.; Legzdins, P.; Trotter, J. *Inorg. Chem.* **1979**, *18*, 3543–3548. (b) Goh, L. Y.; Hambley, T. W.; Robertson, G. B. *J. Chem. Soc., Chem. Commun.* **1983**, 1458–1460. (c) Goh, L. Y.; Hambley, T. W.; Robertson, G. B. *Organometallics* **1987**, *6*, 1051–1057.  
 (39) Beekman, R. A.; Boeré, R. T.; Moock, K. H.; Parvez, M. *Can. J. Chem.* **1998**, *76*, 85–93.  
 (40) SMART & SAINT Software Reference manuals, version 5.0, Bruker AXS Inc., Madison, WI, 1998.  
 (41) Sheldrick, G. M. SADABS software for empirical absorption correction; University of Göttingen: Germany, 2000.  
 (42) SHELXTL Reference Manual, version 5.1, Bruker AXS Inc., Madison, WI 1998.

(36) Ernest, I.; Holick, W.; Rihs, G.; Schomburg, D.; Shoham, G.; Wenkert, D.; Woodward, R. B. *J. Am. Chem. Soc.* **1981**, *103*, 1540–1544.

**Table 1.** Data Collection and Refinement Data

	3a	3b	3c	3d	3e	2d
formula	C <sub>15</sub> H <sub>12</sub> CrN <sub>2</sub> O <sub>2</sub> S <sub>2</sub>	C <sub>14</sub> H <sub>9</sub> CrClN <sub>2</sub> O <sub>2</sub> S <sub>2</sub>	C <sub>15</sub> H <sub>12</sub> CrON <sub>2</sub> O <sub>2</sub> S <sub>2</sub>	C <sub>15</sub> H <sub>9</sub> CrF <sub>3</sub> N <sub>2</sub> O <sub>2</sub> S <sub>2</sub>	C <sub>19</sub> H <sub>17</sub> CrN <sub>3</sub> O <sub>2</sub> S <sub>2</sub>	C <sub>16</sub> H <sub>8</sub> F <sub>6</sub> N <sub>4</sub> S <sub>4</sub>
fw	368.39	388.80	384.39	422.36	435.48	498.50
cryst syst	triclinic	orthorhombic	monoclinic	monoclinic	triclinic	triclinic
space group	<i>P</i> 1	<i>Pbca</i>	<i>P</i> 2 <sub>1</sub> / <i>n</i>	<i>P</i> 2 <sub>1</sub> / <i>c</i>	<i>P</i> 1	<i>P</i> 1
<i>a</i> , Å	7.7225(9)	13.894(2)	9.8511(6)	9.9853(10)	6.3689(15)	9.4916(9)
<i>b</i> , Å	9.7779(11)	10.9981(15)	7.9608(5)	22.019(2)	12.436(3)	18.1887(17)
<i>c</i> , Å	11.7171(13)	19.653(3)	20.1840(12)	7.3781(8)	12.857(3)	22.275(2)
$\alpha$ , deg	67.524(2)	90	90	90	106.480(5)	91.579(1)
$\beta$ , deg	86.123(2)	90	100.1910(10)	104.736(3)	91.552(4)	97.329(1)
$\gamma$ , deg	69.230(2)	90	90	90	92.249(4)	102.755(1)
<i>V</i> , Å <sup>3</sup>	762.05(15)	3003.1(7)	1557.91(16)	1568.8(3)	974.9(4)	3713.8(6)
<i>Z</i>	2	8	4	4	2	8
<i>T</i> , K	223(2)	223(2)	223(2)	223(2)	295(2)	173(2)
$\rho_{\text{calc}}$ , g cm <sup>-3</sup>	1.605	1.720	1.639	1.788	1.483	1.783
$\mu$ , mm <sup>-1</sup>	1.031	1.223	1.017	1.040	0.820	0.583
<i>F</i> (000)	376	1568	784	848	448	2000
$\theta$ , deg	1.89–27.50	2.07–27.50	2.05–27.50	1.85–27.50	1.65–25.00	1.85 to 26.22
index ranges	−10 ≤ <i>h</i> ≤ 10 −12 ≤ <i>k</i> ≤ 12 −15 ≤ <i>l</i> ≤ 15	−18 ≤ <i>h</i> ≤ 12 −14 ≤ <i>k</i> ≤ 14 −25 ≤ <i>l</i> ≤ 21	−12 ≤ <i>h</i> ≤ 9 −10 ≤ <i>k</i> ≤ 10 −26 ≤ <i>l</i> ≤ 26	−12 ≤ <i>h</i> ≤ 7 −28 ≤ <i>k</i> ≤ 27 −9 ≤ <i>l</i> ≤ 9	−7 ≤ <i>h</i> ≤ 6 −12 ≤ <i>k</i> ≤ 14 −15 ≤ <i>l</i> ≤ 15	−11 ≤ <i>h</i> ≤ 11 −22 ≤ <i>k</i> ≤ 22 −27 ≤ <i>l</i> ≤ 27
reflns collect.	10001	19853	10776	11106	5146	39140
unique reflns	3489	3441	3582	3590	3418	14828
data/restr/param	3489/0/200	3441/0/199	3582/0/209	3590/0/226	3418/18/259	14828/18/1089
<i>R</i> indices ( <i>I</i> > 2 $\sigma$ ( <i>I</i> )) <sup>a,b</sup>	R1 = 0.0511 wR2 = 0.1093	R1 = 0.0726 wR2 = 0.1437	R1 = 0.0414 wR2 = 0.0955	R1 = 0.0689 wR2 = 0.1345	R1 = 0.0703 wR2 = 0.1446	R1 = 0.0568 wR2 = 0.1005
<i>R</i> indices (all data)	R1 = 0.0617 wR2 = 0.1139	R1 = 0.0867 wR2 = 0.1490	R1 = 0.0508 wR2 = 0.1002	R1 = 0.0883 wR2 = 0.1414	R1 = 0.1359 wR2 = 0.1690	R1 = 0.1431 wR2 = 0.1272
GOF on <i>F</i> <sup>2</sup> <sup>c</sup>	1.159	1.300	1.072	1.213	0.940	0.990
largest peak, hole, e Å <sup>-3</sup>	0.548, −0.411	0.794, −0.622	0.369, −0.260	0.524, −0.507	0.476, −0.278	0.812, −1.013

<sup>a</sup> R1 =  $(\sum|F_o| - |F_c|)/\sum|F_o|$ . <sup>b</sup> wR2 =  $[(\sum w|F_o| - |F_c|)^2/\sum w|F_o|^2]^{1/2}$ . <sup>c</sup> GOF =  $[(\sum w|F_o| - |F_c|)^2/(N_{\text{observns}} - N_{\text{params}})]^{1/2}$ .

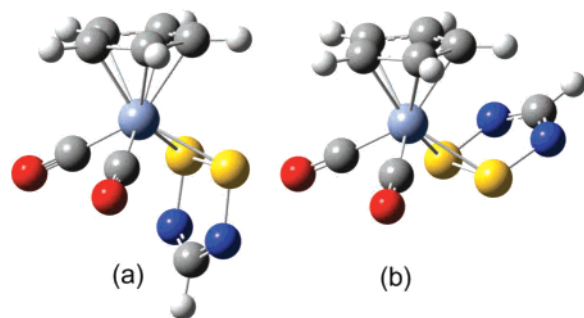


**Figure 1.** Optimized model complexes of (a) exo isomer **2f** (−2409.142 360 2 hartree) and (b) endo isomer **2g** (−2409.143 318 hartree) from B3PW91/6-311+G(2d,2p)//B3PW91/6-31G(d) calculations. Atom codes: Cr, light blue; S, yellow; N, dark blue; O, red; C, gray; H, white. Bond distances and angles for these structures are included in Table 2.

Chemie  $\mu$ Autolab III potentiostat with 1 mm diameter glassy carbon (GC) and Pt working electrodes. Potentials were referenced to the ferrocene/ferrocenium (Fc/Fc<sup>+</sup>) redox couple, which was used as an internal standard. The electrochemical cell was thermostated at 233 and 293 K using an Eyela PSL-1000 variable-temperature cooling bath.

Simultaneous electrochemical electron paramagnetic resonance (SEEP) spectroscopy experiments were conducted in conventional EPR flat cells in a Bruker TE<sub>102</sub> cavity using a modified version of a cell described in the literature based on an Au-micromesh working electrode.<sup>43</sup> The spectrometer was an EMX113/12 model operating in X-band (9.4 GHz) under ambient conditions or at reduced *T* employing the standard Bruker LN<sub>2</sub> cryostat and a miniature EPR flat cell.<sup>44</sup> Solutions of the complex (8.0 mM **3a**, 1.7 mM **3b**, 8.7

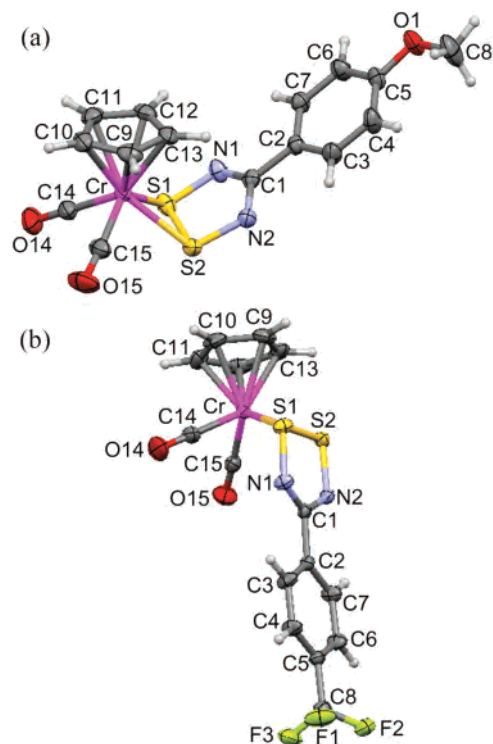


**Figure 2.** Thermal ellipsoid plots showing the molecular structures of (a) endo isomer **3c** and (b) exo isomer **3d** as found in the crystals.

mM **3c**, 3.6 mM **3d**, 4.6 mM **3e**) in CH<sub>3</sub>CN containing 0.1 M *n*-Bu<sub>4</sub>NPF<sub>6</sub> were loaded into the flat cell (ca. 2 mL), and background EPR spectra were obtained. Subsequently cyclic voltammograms were obtained in situ, and the potential was adjusted to the anodic (oxidation) or cathodic (reduction) peak potentials. Single scans of 40 or 80 s were obtained simultaneous with electrolyses of the same duration. Radical lifetimes were determined by setting the

(43) (a) Boeré, R. T.; Bond, A. M.; Chivers, T.; Feldberg, S. W.; Roemmele, T. L. *Inorg. Chem.* **2007**, *46*, 5596–5607. (b) Neudeck, A.; Kress, L. *J. Electroanal. Chem.* **1997**, *437*, 141–156.

(44) Boeré R. T.; Roemmele, T. L. In preparation.

**Table 2.** Metric Data from Crystallography and DFT Calculation

	3a <sup>a</sup>	3b <sup>a</sup>	3c <sup>a</sup>	3d <sup>a</sup>	3e <sup>a</sup>	3f <sup>b</sup>	3g <sup>b</sup>
isomer	exo	endo	endo	exo	endo	exo	endo
Bond Distance (Å)							
Cr(1)–S(2)	2.3454(9)	2.3537(12)	2.3407(7)	2.3505(12)	2.361(2)	2.3721	2.3878
Cr(1)–S(1)	2.3463(9)	2.3602(13)	2.3688(7)	2.3334(12)	2.3540(19)	2.3721	2.3878
S(1)–N(1)	1.640(3)	1.642(4)	1.640(2)	1.642(4)	1.636(5)	1.6478	1.6542
S(1)–S(2)	2.1143(10)	2.1315(15)	2.1487(9)	2.1280(15)	2.146(3)	2.2108	2.2021
S(2)–N(2)	1.644(2)	1.635(4)	1.641(2)	1.627(3)	1.632(5)	1.6478	1.6542
N(1)–C(1)	1.340(4)	1.337(5)	1.333(3)	1.330(5)	1.335(7)	1.3301	1.3290
N(2)–C(1)	1.332(4)	1.333(6)	1.338(3)	1.340(5)	1.329(8)	1.3301	1.3290
Bond Angle (deg)							
S(2)–Cr(1)–S(1)	53.57(3)	53.77(4)	54.29(2)	54.04(4)	54.14(7)	55.55	55.04
N(1)–S(1)–S(2)	94.77(9)	93.79(13)	93.31(8)	93.48(13)	93.3(2)	92.63	92.77
N(1)–S(1)–Cr(1)	114.76(10)	112.62(14)	111.87(8)	114.91(13)	110.99(19)	112.99	112.81
S(2)–S(1)–Cr(1)	63.19(3)	62.96(4)	62.19(2)	63.39(4)	63.10(7)	62.22	62.48
N(2)–S(2)–S(1)	93.62(9)	93.79(14)	93.53(8)	94.35(13)	93.5(2)	92.63	92.77
N(2)–S(2)–Cr(1)	113.17(9)	114.00(14)	113.08(7)	115.49(13)	112.6(2)	112.99	112.81
S(1)–S(2)–Cr(1)	63.24(3)	63.27(4)	63.52(2)	62.57(4)	62.76(7)	62.22	62.48
C(1)–N(1)–S(1)	113.3(2)	114.2(3)	114.88(17)	114.3(3)	114.5(4)	114.23	114.22
C(1)–N(2)–S(2)	114.3(2)	114.6(3)	114.39(17)	114.0(3)	114.5(4)	114.23	114.22

<sup>a</sup> Full geometrical details are provided in the CIF files. <sup>b</sup> From B3PW91/6-311+G(2d,2p)/B3PW91/6-31G(d) calculations within *C*<sub>2v</sub> symmetry.

EPR field at the signal center and scanning in the time dimension, first setting a baseline and then commencing electrolysis until maximum signal intensity was obtained, stopping electrolysis and monitoring the decay of the signal. First-order decay curves were fitted to exponential decay (correlation coefficient  $\geq 0.99$ ). The reported EPR parameters were obtained from complete digital line-fitting routines using WinSim 2002.<sup>45</sup>

**2.6. Hybrid DFT Calculations.** The structures of diamagnetic adducts  $\eta^5$ -CpCr(CO)<sub>2</sub>( $\eta^2$ -S<sub>2</sub>N<sub>2</sub>CH) in exo (**3f**) and endo (**3g**) conformations were optimized with *C*<sub>s</sub> symmetry in their ground states using density functional theory in the Gaussian 98W suite of programs.<sup>46</sup> The B3PW91 functional<sup>47</sup> with the 1991 gradient-corrected correlation functional of Perdew and Wang<sup>48</sup> was used; this hybrid functional has previously been shown to provide realistic geometries for organochromium complexes.<sup>49</sup> The Gaussian basis set 6-31+G(d) was used for geometry optimization and 6-311+G-(2d,2p) for the final energy calculations. The computed structures are illustrated in Figure 1, while Table 2 includes the calculated bond distances and angles. A more complete list of geometrical parameters is shown in Figure S6.

**2.7. Dynamic NMR Experiments.** The <sup>1</sup>H spectra obtained from 200 to 300 K were subjected to line shape analysis using both the Cp and aromatic signals. The Cp signal was treated as a two-site, one-spin-1/2, unequally populated, exchange system including transverse relaxation for both sites. Spectra were simulated using an implementation of the McConnell<sup>50</sup> formalism in Matlab.<sup>51</sup> In this approach the Bloch equations are modified to include chemical exchange but do not include weak coupling effects. The aromatic region was treated as an unequally populated two-site four-spin system. This system was treated using a time-dependent quantum mechanics approach utilizing the density matrix.<sup>52</sup> The aromatic spin systems on both sites were assumed to be AA'BB'. This density matrix treatment was also implemented in Matlab. Both analyses used chemical shifts, scalar couplings, and transverse relaxation

times as input parameters for each nucleus along with the equilibrium constant and exchange rate.

For each temperature, candidate spectra were computed for particular chemical shifts, scalar couplings, relaxation times, equilibrium constants, and the rate constants, and these were compared visually with the experimental traces. The rate constant was changed until an optimal match was achieved. Values for the equilibrium constant, chemical shift, and relaxation times were obtained by extrapolating measurements from the lower temperatures where chemical exchange effects do not interfere with the measurements. In this manner, determinate error due to temperature drift in these parameter can be removed, greatly increasing the accuracy of the rate measurements.<sup>53</sup> Errors in the rate measurements were estimated by perturbing the rate until differences with the experimental spectrum became apparent. We estimate that rate measurements accurate to within 10% are achieved.<sup>53</sup> The activation parameters for each data set were determined from the rate measurements using the Eyring equation. The activation enthalpy was obtained from the slope and the activation entropy from the intercept.<sup>54,55</sup> Similarly the enthalpy and entropy difference between the two isomers was obtained from the equilibrium constants using the temperature dependence of the Gibbs energy. A complete set of the spectral changes and line-fits are provided in Figures S1–S3 of the Supporting Information. The original equilibrium and rate data as well as the Eyring plots are provided in Tables S1 and S2 and Figures S4 and S5 of the Supporting Information. Summary data extracted from the fits is presented in Table S3 of the Supporting Information.

### 3. Results and Discussion

**3.1. Reaction of Cyclopentadienylchromium Tricarbonyl Dimer, [CpCr(CO)<sub>3</sub>]<sub>2</sub> (1), with 1,2,3,5-Dithiadiazolyl Dimers in Equimolar Ratios.** The reactions of [CpCr(CO)<sub>3</sub>]<sub>2</sub> (1) with 1 mol equiv of (4-R-C<sub>6</sub>H<sub>4</sub>CN<sub>2</sub>S<sub>2</sub>)<sub>2</sub> (R = Me, **2a**;

(45) WinSim (v.0.98, 2002) software: Duling, D. R. *J. Magn. Reson. B* **1994**, *104*, 105–110.

(46) Frisch, M. J.; et al. *Gaussian 98W*, revision A.9; Gaussian, Inc.: Pittsburgh, PA, 1998.

(47) Becke, A. D. *J. Chem. Phys.* **1993**, *98*, 5648–5652.

(48) Perdew, J. P.; Wang, Y. *Phys. Rev. B* **1992**, *45*, 13244–13249.

(49) Carlson, C. N.; Smith, J. D.; Hanusa, T. P.; Brennessel, W. W.; Young, V. G., Jr. *J. Organomet. Chem.* **2003**, *683*, 191–199.

(50) McConnell, H. M. *J. Chem. Phys.* **1956**, *28*, 430–431.

(51) Mathworks, Inc. Matlab 6.5, 2002.

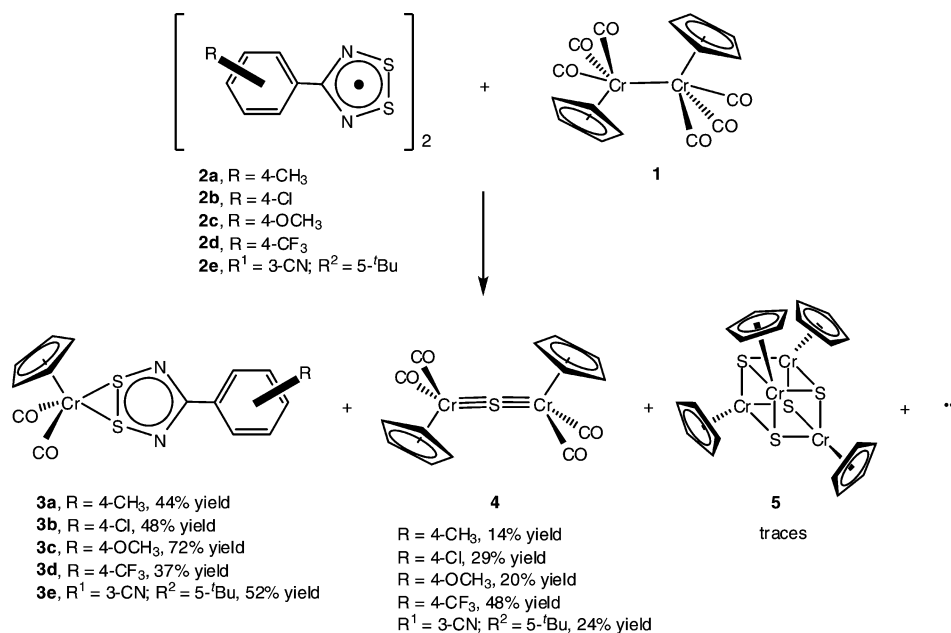
(52) Fano, U. *Rev. Mod. Phys.* **1957**, *29*, 74–93.

(53) (a) Bain, A. D.; Cramer, J. A. *J. Phys. Chem.* **1993**, *97*, 2884–2887. (b) Bain, A. D.; Cramer, J. A. *J. Magn. Reson. A* **1993**, *103*, 217–222.

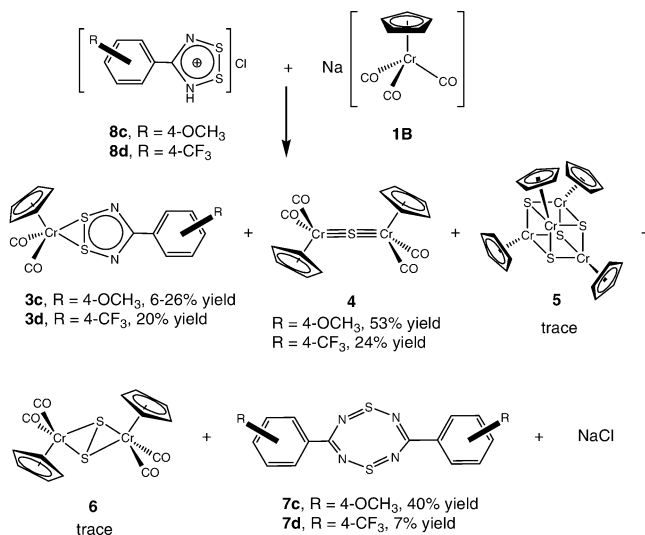
(54) Bain, A. D.; Duns, G. J.; Ternieden, S.; Ma, J.; Werstuijk, N. H. *J. Phys. Chem.* **1994**, *98*, 7458–7463.

(55) For data sets obtained over large temperature ranges, errors in the enthalpy can be as small as 1 kJ/mol and in the entropy as small as 5 J/mol K: Bain, A. D.; Hazendonk, P. *J. Phys. Chem. A* **1997**, *101*, 7182–7188.

Scheme 2



Scheme 3



Cl, **2b**; OMe, **2c**; CF<sub>3</sub>, **2d**; 3-CN, 5-<sup>t</sup>Bu, **2e**) in toluene at ambient temperature led to the isolation of deep-green crystals of [CpCr(CO)<sub>2</sub>]<sub>2</sub>S (**4**) and fine red crystalline solids of CpCr(CO)<sub>2</sub>(η<sup>2</sup>-S<sub>2</sub>N<sub>2</sub>CC<sub>6</sub>H<sub>4</sub>R) [R = 4-Me, **3a**; 4-Cl, **3b**; 4-OMe, **3c**; 4-CF<sub>3</sub>, **3d**] and CpCr(CO)<sub>2</sub>(η<sup>2</sup>-S<sub>2</sub>N<sub>2</sub>CC<sub>6</sub>H<sub>3</sub>-3-(CN)-5-(<sup>t</sup>Bu)) (**3e**) in yields shown in Scheme 2.

<sup>1</sup>H NMR tube reactions showed that (i) using 2 mol equiv of **1** to **2** gave higher yields of **4**, together with two other unidentifiable byproducts possessing δ(Cp's) 4.48 and 4.51, with relative molar ratio being, respectively 14:1:2:10 (for **3a**). (ii) **3a** reacted readily with one mol equiv of **1** at ambient temperature, undergoing 25% conversion to **4** after 2.5 h. (iii) With 2 mol equiv of **1**, **3a** was more than 90% transformed after a day to **4**, **5**, and the unknowns "δ 4.48" and "δ 4.51" in relative molar proportion of 200:5:1:7. These NMR experiments confirm that a most probable route to **4** is the interaction of the primary product **3a** or **3b** with an excess of **1**, resulting in S-abstraction from the coordinated

heterocyclic ring of dithiadiazolyls. Indeed, our previous work had demonstrated the role of **1A** as a strong thiophile, capable of abstracting S from various classes of S-containing ligands at a CpCr center, leading to partially or fully *desulfurized* derivatives.<sup>7,12</sup> Unfortunately in this particular case, we were unable to isolate the resulting metal complex or organic products nor obtain any clear indication of their presence in NMR spectral analysis of the solution of total crude products.

**3.2. Reaction of Sodium Cyclopentadienylchromium Tricarbonyl, Na[CpCr(CO)<sub>3</sub>] (**1B**), with 1,2,3,5-Dithiadiazolium Chlorides.** The very rapid reactions of Na[CpCr(CO)<sub>3</sub>] (**1B**) with 1 mol equiv of 4-R-C<sub>6</sub>H<sub>4</sub>CN<sub>2</sub>S<sub>2</sub>Cl (R = OMe, **8c**; CF<sub>3</sub>, **8d**) in toluene/THF at -29 °C led to the isolation of 3,7-(4-R-C<sub>6</sub>H<sub>4</sub>)<sub>2</sub>{CN<sub>2</sub>S<sub>2</sub>N<sub>2</sub>C} (R = OMe, **7c**, 40%; CF<sub>3</sub>, **7d**, 7%) and fine red crystalline solids of CpCr(CO)<sub>2</sub>(η<sup>2</sup>-S<sub>2</sub>N<sub>2</sub>CC<sub>6</sub>H<sub>4</sub>R) (R = OMe, **3c**, 6%; CF<sub>3</sub>, **3d**, 20%), along with **4-6** and NaCl shown in Scheme 3. The lower yields of **3c** and **3d** here obtained as compared with those from the radical reactions were unexpected, as higher yields were anticipated from this direct metathetic salt elimination reaction. This observation may be ascribed to the high thermal instability of the complexes **3c**, which readily transforms to **5** via **4**. Indeed, in an NMR tube study, complex **3c** could only be detected in the product mixture from a reaction at -30 °C; at ambient temperature **4** was the predominant product. It may be plausible that the exothermic heat of formation of NaCl in the "salt" reaction contributed to the degradation of complexes **3**. However, though this may be substantiated by a comparison of the relative yield of **4:3c** in the radical and salt reactions, the same inference cannot be drawn in the case of **3d**, wherein the **4:3d** yield ratio remains relatively unchanged in both types of reactions.

A more likely mechanism would involve a prior redox reaction between [CpCr(CO)<sub>3</sub>]<sup>-</sup> (**1B**) and [RC<sub>6</sub>H<sub>4</sub>CN<sub>2</sub>S<sub>2</sub>]<sup>+</sup>

(**8c,d**), generating the radical species, CpCr(CO)<sub>3</sub><sup>•</sup> (**1A**) and RC<sub>6</sub>H<sub>4</sub>CN<sub>2</sub>S<sub>2</sub><sup>•</sup> (**2A**), which then couple to form **3**, as in the reaction between the dimeric species. This postulate is supported by electrochemical data, which shows that these two systems are “redox-incompatible”,<sup>56</sup> the redox potentials ( $E_{1/2}$ ) vs SCE being +0.57 V (**8c**, R = 4-OMe) and +0.66 V (**8d**, R = 4-CF<sub>3</sub>) for [RC<sub>6</sub>H<sub>4</sub>CN<sub>2</sub>S<sub>2</sub>]<sup>+•57</sup> and -0.28 V for [CpCr(CO)<sub>3</sub>]<sup>•-58</sup>. Thus, the strongly oxidizing property of **8c,d** in concert with the strongly reducing property of **1B** provides the driving force for a redox reaction that generates the corresponding radical precursors **2A** and **1A** to complexes **3**.<sup>56</sup> Support for the above postulate is provided by the isolation of the dithiatetrazocines **7c,d**, which are known oxidation products of the free radicals.<sup>34a</sup> Structurally it is evident that these arise from coupling of the desulfurized derivative RC<sub>6</sub>H<sub>4</sub>CN<sub>2</sub>S<sup>•</sup> of **2A**, which by inference and inter alia must have been present in this “salt” reaction. On the basis of our observation of the sluggish reaction of **1B** with S<sub>8</sub> to give **4** in 7% yield versus quantitative yield in the facile analogous reaction of **1/1A**,<sup>38b,c</sup> the obtained high yields of **4** in this reaction (53 and 24%) also argues against the anion **1B** being the active reagent, and supports the intermediary role of the radical **1A**.

**3.3. Crystal Structure and Spectroscopic Analyses.** The molecular structures of these complexes show that the coordination geometry at Cr is similar, with Cr atoms assuming a four-legged piano-stool configuration, being bonded to a bidentate (S,S) dithiadiazolyl ligand and two CO ligands. However, the relative orientations of the heterocyclic ligands are very different. The dithiadiazolyl ligand of **3a** and **3d** is orientated toward the CO ligands, away from the Cp ring (exo configuration), while that of **3b**, **3c**, and **3e** is orientated away from the CO ligands, and toward the Cp ring (endo configuration). The hinge angles at the S–S bonds between the CrS<sub>2</sub> and S<sub>2</sub>N<sub>2</sub> planes are +65.2° in **3a**, -65.7° in **3b**, -66.5° in **3c**, +63.6° in **3d**, and -67.2° in **3e**. Torsion angles between the S<sub>2</sub>N<sub>2</sub>C and aryl rings vary from 3° to 16°. The molecular structures for an endo isomer (**3c**) and an exo isomer (**3d**) are depicted in Figure 2. Selected metric data of all five structures are given in Table 2.

While there are many reported structures for dithiadiazolyls in the literature, of those employed here, only **2c**<sup>59</sup> and **2e**<sup>34b</sup> have been reported previously. We report the structure of **2d** for the first time. While many dithiadiazolyls undergo phase transitions on cooling that affect crystallinity, we were able to obtain a structure for **2d** at 173 K. A typical cis-cofacial<sup>26</sup> dimer structure is displayed in Figure 3.<sup>60</sup> The molecule shows evidence of distortion to accommodate the

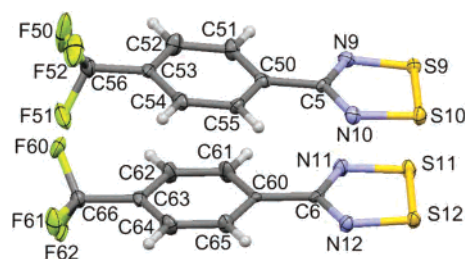


**Figure 3.** Thermal ellipsoids plot of one of the four cis-cofacial dimers found in the crystal structure of **2d**. In this particular dimer,  $d(\text{S9}\cdots\text{S11}) = 3.054 \text{ \AA}$  and  $d(\text{S10}\cdots\text{S12}) = 3.031 \text{ \AA}$ . The average  $d(\text{S}-\text{S}) = 2.083(5) \text{ \AA}$ ,  $d(\text{S}-\text{N}) = 1.629(7) \text{ \AA}$ , and  $d(\text{N}-\text{C}) = 1.337(4) \text{ \AA}$  over all eight monomers (errors are standard deviations).

bulky para CF<sub>3</sub> groups, so that, for example, the two interannular S<sup>•••</sup>S contacts are quite dissimilar. The association of dithiadiazolyls in this fashion has been convincingly attributed to diffuse  $\pi^*-\pi^*$ -interactions between the two ring SOMOs,<sup>61</sup> as indicated by interannular S<sup>•••</sup>S distances being considerably longer than the Cr–S distances in **3** (see below).

In the metal complexes, the CN<sub>2</sub>S<sub>2</sub> ring of the heterocyclic ligand remains intact, with only some lengthening (ca. 2%) of the S–S bond upon coordination [2.1143(10) Å in **3a**, 2.1315(15) Å in **3b** versus 2.103(5) Å in unligated **2b** at room temperature,<sup>59</sup> 2.1487(9) Å in **3c**, 2.1280(15) Å in **3d** versus an average 2.083(5) Å over eight unique molecules of **2b** at 173 K and 2.146(3) Å in **3e** versus 2.101(2) in **2e**],<sup>34b</sup> while the C–N and S–N bonds remain virtually unchanged [ca. 1.330–1.340 and 1.627–1.644 Å, respectively, versus 1.337(4) and 1.629(7) Å in the free ligand **2d**, for instance]. There thus exists a strained three-membered CrS<sub>2</sub> ring, with a small S–Cr–S bond angle [53.57(3)° in **3a**, 54.29(2)° in **3c**]. These angles are larger than those in Cp<sub>2</sub>Cr<sub>2</sub>(CO)<sub>4</sub>( $\mu-\eta^2$ -S<sub>2</sub>) [48.8(0)° and 49.0(0)°] and in Cp<sub>2</sub>Cr<sub>2</sub>(CO)<sub>5</sub>( $\mu-\eta^1, \eta^2$ -S<sub>2</sub>) [50.1(1)°], which undoubtedly are related to the shorter S–S bonds of 1.990(1) and 2.010(4) Å, respectively,<sup>38c</sup> but they are, as expected, smaller than the “open” S–Cr–S angles (70.3°–83.65°) found in CpCr(CO)<sub>2</sub> complexes

(56) We use the term *redox compatible* to mean species with overlapping redox stability windows, for which the driving force for an immediate electron transfer reaction is absent: Ang, C. W.; Boeré, R. T.; Goh, L. Y.; Koh, L. L.; Kuan, S. L.; Tan, G. K.; Yu, X. *Chem. Commun.* **2006**, 4735–4737.

(57) Boeré, R. T.; Roemmele, T. L. *Coord. Chem. Rev.* **2000**, *210*, 369–445.

(58) Barbini, D. C.; Tanner, P. S.; Francone, T. D.; Furst, K. B.; Jones, W. E. *Inorg. Chem.* **1996**, *35*, 4017–4022.

(59) Boeré, R. T.; Mooock, K. H.; Parvez, M. Z. *Anorg. Allg. Chem.* **1994**, *620*, 1589–1598.

(60) The unit cell of **2d** contains eight monomeric F<sub>3</sub>CC<sub>6</sub>H<sub>4</sub>CN<sub>2</sub>S<sub>2</sub> rings in the asymmetric unit (Figure S8), each arranged to give four distinct cis-cofacial dimers, each of which has a different manifestation of steric distortion to accommodate the bulky CF<sub>3</sub> group. These dimers associate in two zones within the lattice: in the first, four dimers aggregate around an approximate four-fold axis in a “pin-wheel” motif that has been observed previously for DTDA structures. In the second, six dimer pairs align side-by-side in sets of three. In each case, there are short cross-ring S<sup>•••</sup>N interactions. In addition, there are considerably longer S<sup>•••</sup>S and S<sup>•••</sup>N contacts in the stacking direction. Such complexity has been seen previously in DTDA crystal structures, with two of the 45 reported neutral DTDA structures contained in the CSD (V 5.28, 2007) having the same number of monomers per equivalent position. Specifically, a long-known structure of CH<sub>3</sub>CN<sub>2</sub>S<sub>2</sub> crystallizes in the same space group as **2d**: Banister, A. J.; Hansford, M. I.; Hauptman, Z. V.; Wait, S. T.; Clegg, W. *J. Chem. Soc., Dalton Trans.* **1989**, 1705–1713. A more recently reported polymorph of ClCN<sub>2</sub>S<sub>2</sub>—which like **2d** was collected at low temperature—crystallizes in P2<sub>1</sub>/c: Bond, A. D.; Haynes, D. A.; Pask, C. M.; Rawson, J. M. *J. Chem. Soc., Dalton Trans.* **2002**, 2522–2531. The closely related compound 4-CF<sub>3</sub>-3-F-C<sub>6</sub>H<sub>3</sub>CN<sub>2</sub>S<sub>2</sub> shows similar steric distortions as found in **2c**, though it crystallizes with only four monomers per equivalent position in P1: Clarke, C. S.; Haynes, D. A.; Rawson, J. M.; Bond, A. D. *Chem. Commun.* **2003**, 2774–2775. As commonly observed in such structures, the dominant local pairing into dimers—a manifestation of the Peierls distortion—prevents the long-range contacts essential for a conducting state.

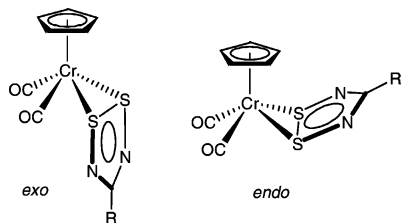
(61) Oakley, R. T. *Prog. Inorg. Chem.* **1988**, *36*, 299–391.

containing bidentate  $S_2PPh_2$ ,<sup>3</sup>  $S_2P(O^iPr)_2$ ,<sup>4</sup>  $S_2CNR_2$ ,<sup>5b</sup> and  $S_2CO^iPr$  ligands.<sup>62</sup> The Cr–S bond lengths [range 2.3334(12)–2.3688(7) Å] lie at the low end of the range previously observed for other CpCr complexes, viz. 2.348(2)–2.466(2) Å for complexes containing bare S ligands,<sup>38c</sup> 2.321(4)–2.517(3) Å for complexes containing bare P/S ligands,<sup>8</sup> 2.365(1)–2.471(3) Å for complexes containing bridging SPh ligands,<sup>2a</sup> and 2.3711(8)–2.517(8) Å for complexes containing  $S_2PR_2$  or  $S_2P(OR)_2$ .<sup>3–4</sup>

The bonding mode in **3a–e** is new for dithiadiazolyl metal chemistry. To date, transition metal complexes or their fragments have always cleaved the S–S bond of the heterocyclic ring (see examples in Chart 2). In these cases, the reported S···S distances fall between 2.91 and 3.17 Å,<sup>19–26</sup> consistent with almost zero bond order according to the estimated values of 2.03 and 1.60 Å for the effective radii of sulfur, perpendicular to and along the bond.<sup>63</sup>

Considering the formal uninegative charges of the Cp and dithiadiazolyl ligands<sup>64</sup> and the overall neutrality of the complexes, the Cr centers can be considered to be in +2 oxidation state. With the heterocyclic ligand as a three-electron donor, the 18-electron rule is obeyed in each of the complexes, and this is reflected in their predominantly diamagnetic nature as indicated in their proton NMR spectra.

The molecular structures of these complexes are supported by their IR, NMR, and mass spectral data. The IR spectra possess two terminal CO stretches. The  $^1H$  NMR spectra show for **3a**,  $\delta(Cp)$  3.86 and  $\delta(Me)$  2.00; for **3b**,  $\delta(Cp)$  3.80; for **3c**,  $\delta(Cp)$  3.86 and  $\delta(OMe)$  3.18; for **3d**,  $\delta(Cp)$  3.79; and for **3e**,  $\delta(Cp)$  3.78, together with broad unresolved multiplets for the aryl protons in all cases. The parent ions  $[M + 1]^+$  are seen in their  $FAB^+$ -mass spectra.



**3.4. Dynamic  $^1H$  NMR Study of **3d**.** The discovery of endo and exo conformations in different derivatives of **3** in the solid-state caused us to examine their solution  $^1H$  NMR spectra carefully; in each case, only one set of signals due to **3** occurs in room temperature spectra in benzene- $d_6$  (see Experimental Section), with the expected singlet from Cp and two aromatic AA' and BB' doublets for **3a–d** and three distinct aromatic peaks for **3e**. However, for each compound at least one of the aromatic signals was line-broadened at room temperature, indicative of dynamic processes in solution. Therefore, we carried out a variable-temperature  $^1H$

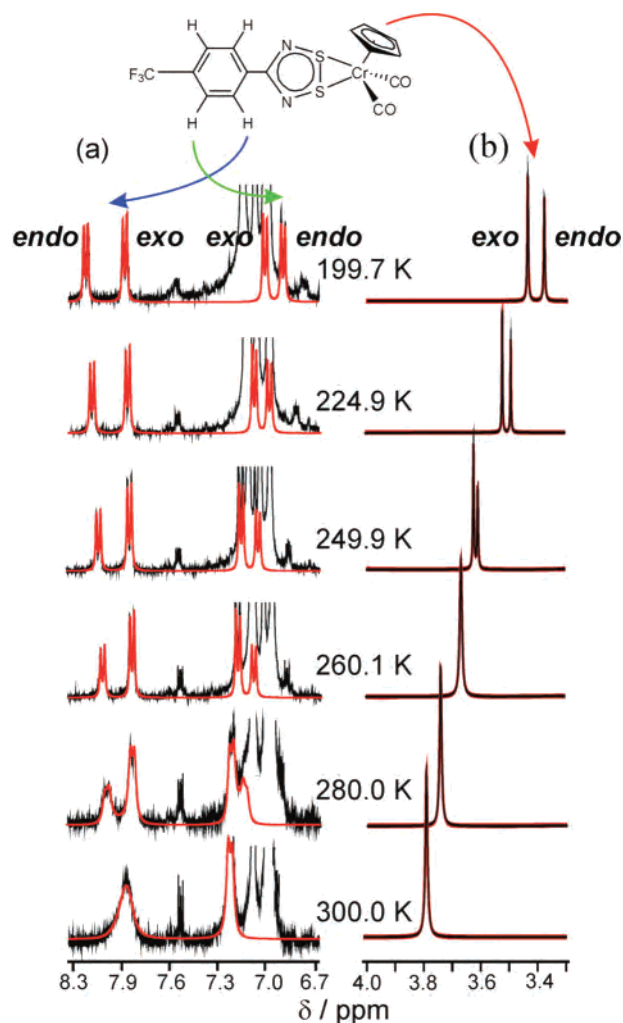


**Figure 4.** Stacked plots of  $^1H$  NMR traces in (a) the AA'BB' aromatic and (b) the Cp regions of **3d** over the range 200–300 K, showing every second temperature measured. Experimental data in black; computed spectra from line-shape fitting in red. Unfitted lines are either due to the residual toluene- $d_8$  signals or minor impurities. The aromatic region has a much increased vertical scale, the more so at high temperature where coalescence broadening occurs; the rms noise in the baseline of parts a and b is identical.

NMR experiment in toluene- $d_8$  on the most soluble exemplar available to us, complex **3d** (an exo isomer in the crystal). On cooling, complex spectral changes occur in this system (Figures 4 and S1).

Both the aromatic and Cp signals separate at different temperatures into two sets of signals. The population of the two interchanging species is strongly temperature dependent ( $K = [endo]/[exo]$  ranges from  $\sim 0.6$  at room temperature to  $\sim 0.9$  at 200 K), and their chemical shifts are also strongly temperature dependent [thus average  $\delta(Cp)$  moves 0.37 ppm to higher field; average  $\delta(AA')$  aromatic set by 0.13 and  $\delta(BB')$  by 0.10 ppm to lower field on cooling from room temperature to 200 K].

First, we attempt to assign the spectra. From considerable experience with disubstituted aryl groups attached to thiazyl rings, we can confidently assign the broad aryl  $^1H$  resonance at  $\sim \delta$  8.0 ( $\nu_{1/2} = 14$  Hz) in the room temperature spectrum to the benzene hydrogen atoms ortho to the  $CN_2S_2$  ring and hence the  $\delta$  (7.25) set to the meta atoms. For example, in **3e** the two broadened signals occur at  $\delta$  8.36 and 8.16. We note

(62) Ng, V. W. L.; Kuan, S. L.; Weng, Z.; Leong, W. K.; Vittal, J. J.; Koh, L. L.; Tan, G. K.; Goh, L. Y. *J. Organomet. Chem.* **2005**, *690*, 2323–2332.

(63) Nyburg, S. C.; Faerman, C. H. *Acta Crystallogr., Sect. B* **1985**, *41*, 274–279.

(64) The existence of the  $8\pi$  anion has only been demonstrated electrochemically on the time-scale of cyclic voltammetry; see ref 57.

that the lower-population isomer at 200 K displays its Cp resonance 0.11 ppm to *higher* field of the higher-intensity signal, and its AA' aromatic signals 0.5 ppm to *lower* field of the other AA' signal, with a smaller but opposite shift for BB'. We think the most likely cause of these differential shifts is the presence of ring-current effects in the endo isomer that are largely absent in the exo isomer. On the assumption that the aryl-CN<sub>2</sub>S<sub>2</sub> bond is in rapid rotational exchange, the aryl protons will experience in-plane shielding from the aromatic Cp ring, an effect that is expected to operate on the ortho hydrogens, whereas the meta hydrogens experience weak anisotropic shielding as a consequence of geometry. Additionally, the Cp H atoms will experience strong out-of-plane shielding from the aromatic CN<sub>2</sub>S<sub>2</sub> rings in these complexes. Hence, we assign the most shielded Cp and most deshielded aromatic signals to the endo isomer, the species with the lower population in solution at RT. The dynamic nature of all these signals makes confirmation of the assignment by NOESY unfeasible.

Complete line fitting was performed on both the Cp and AA'BB' aryl regions of the <sup>1</sup>H NMR spectrum of **3d** over the range 200–300 K (Figure 4). From the integration of the signals due to the two isomers we have measured the equilibrium constants, and hence rates, for the process



and from the inverse log *K* vs 1/*T* plots, we extracted  $\Delta H^\circ$  and  $\Delta S^\circ$ . From an average of the analyses from the two spectral regions, we obtain  $\Delta H^\circ = -3 \pm 1 \text{ kJ mol}^{-1}$  and  $\Delta S^\circ = -15 \pm 1 \text{ J K}^{-1} \text{ mol}^{-1}$ , indicating that the preference for exo above 190 K is entropically driven and that the endo isomer is enthalpically slightly more stable.

Of greater interest are the activation parameters for the conversion of the two isomers. The line width data were available over a relatively small temperature range, imposed by solvent melting point and the analyte's thermal stability. Moreover, dynamic effects on the line shapes occur in this system over only about a 40 K range. As a result, it was not possible to obtain uncorrelated  $\Delta H^\ddagger$  and  $\Delta S^\ddagger$  values, so that only the free energy of activation can be reported. There is good agreement in  $\Delta G^\ddagger$  between the analyses on the Cp and aromatic signals, with  $\Delta G_{298}^\ddagger = 59 \pm 4 \text{ kJ mol}^{-1}$ . The statistical analysis for the data from the Cp signals indicates a much smaller error in this parameter (see Table S3 for the original data); however, from previous experience, the error in  $\Delta H^\ddagger$  is typically  $\pm 1 \text{ kJ mol}^{-1}$  and in  $\Delta S^\ddagger \pm 5 \text{ J K}^{-1} \text{ mol}^{-1}$ .<sup>55</sup> At 298 K, these estimates would predict an error of  $1.8 \text{ kJ mol}^{-1}$  in  $\Delta G^\ddagger$ , about half of the variance we observe among the two data sets.

We now consider possible mechanisms for exo/endo conversion. Among various conceivable intramolecular processes, a variant on the classic organometallic "ring-whizzing" mechanism, in which there is rotation about the centroid of the S–S bond, shows a much lower barrier than a "hinge" mechanism, which flips the ligand ring about a stationary S–S bond, according to semiempirical PM3-TM calculations. However, exo/endo exchange may also be

**Table 3.** Average Bond Distances (Å) Compared to DFT Calculations

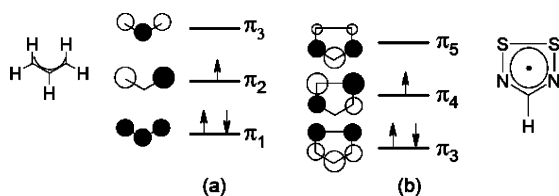
	exo		endo		both
	expt <sup>a</sup>	calc <sup>b</sup>	expt <sup>a</sup>	calc <sup>b</sup>	expt <sup>a</sup>
Cr–S	2.344(1)	2.372	2.356(1)	2.388	2.351(1)
S–S	2.121(1)	2.211	2.142(1)	2.202	2.134(2)
S–N	1.638(3)	1.648	1.638(4)	1.654	1.638(4)
N–C	1.336(4)	1.330	1.334(6)	1.329	1.335(5)

<sup>a</sup> Average over all indicated crystallographic values; errors are root mean squares. <sup>b</sup> From B3PW91/6-311+G(2d,2p)//B3PW91/6-31G(d) calculations within C<sub>2v</sub> symmetry

dissociative, a notion that accords well with the intrinsic stability of both radicals **1A** and **2A**. The strong temperature dependence of the Cp and meta aromatic proton chemical shifts does suggest the presence of small but increasing amounts of a paramagnetic species with a rise in temperature. These shift effects are reversible and, if due to dissociation, the amount of paramagnetic species remains small and in fast exchange at all temperatures, which suggests a very small barrier but a large  $\Delta H^\circ$ . (EPR studies, see below, support the notion that the amount of dissociation is very small). Hence these limited data suggest that both an intramolecular process (e.g., ring-whizzing), with an appreciable barrier but small enthalpy difference, and dissociation, with a very low barrier but a large enthalpy difference, operate simultaneously. The DNMR results thus support the notion that **3d** exists as endo and exo isomers in solution, with the exo configuration thermodynamically favored at room temperature, but with the endo having the lower internal energy. We believe similar effects operate for **3a–e** and attribute the distribution of isomers in the crystal structures that we obtained to either crystal packing forces favoring a given isomer or to fortuitous crystal picking from among a mixture.

**3.5. Structure and Bonding. Hybrid DFT Calculations and Comparison to Allyl Complexes.** Both calculation and the crystallographic measurements seem to indicate a distinct difference in bond lengths between the exo and endo isomers within the CrS<sub>2</sub>N<sub>2</sub>C coordinated rings. Averaged bond distances over the five crystal structures are compiled in Table 3 for ease of comparison with the B3PW91/6-31G(d) calculated values. The errors reported here are root-mean-squares of the individual values from the crystallographic least-squares refinements. The average Cr–S and S–S distances are both shorter in the exo isomers within these experimental errors, although the difference is less than 1%. On the other hand, the S–N and N–C distances are not distinguishable within experimental errors. The DFT-calculated values differ by similar amounts between the two isomers, but most of the computed distances are longer than the measured values by more than the difference between isomers. Curiously, the endo isomer **3g** is calculated to be more stable than the exo isomer **3f** by 2.5 kJ/mol in the gas phase at the B3PW91/6-311+G(2d,2p)//B3PW91/6-31G(d) level of theory, possibly because other bond lengths in the molecule are stabilized in **3g** sufficiently to compensate for the longer distances within the CrS<sub>2</sub>N<sub>2</sub>C moiety. This difference in stability is, however, small in comparison to well-documented limitations on the accuracy of the theoretical methods employed. Thus, while DFT cannot distinguish

Scheme 4



reliably between the stability of the two isomers, the solution-phase NMR data for **3d** also support the notion that the endo isomer is the enthalpically more stable, at least insofar as the NMR assignment is correct. The important point is that both isomers are entirely feasible and apparently bind to the Cr atom with very similar bond types and bond energies.

These calculations also provide insight into the formal resemblance between the bonding of dithiadiazolyls with  $\text{CpCr}(\text{CO})_2$  and  $\pi$ -allyl complexes [note that the directly analogous  $\pi$ -allyls to **3**,  $\text{CpCr}(\text{CO})_2[\text{R}_2\text{CC}(\text{R})\text{CR}_2]$ , have only recently been characterized].<sup>65</sup>

Consideration of the frontier  $\pi$ -orbitals of (a) the allyl radical and (b) the highest three of  $\text{HCN}_2\text{S}_2$  (Scheme 4) emphasizes the similarity between the two systems. Topologically,  $\pi_4$  of the dithiadiazolyl resembles allyl  $\pi_2$ , while  $\pi_3$  of the heterocycle resembles allyl  $\pi_1$ . The separation between the terminal C atoms of the allyl at  $\sim 2.4$  Å is only a little larger than the  $\sim 2.1$  Å between the two sulfur atoms of the dithiadiazolyl, and the p-orbitals of the latter are expected to have larger effective radii, further minimizing the effect of any differences in ligand size. Energetically, these two pairs of orbitals are also similar, while the lower  $\pi$ -orbitals of the heterocycle are of no consequence in metal binding due to the high effective electronegativity of both nitrogen and sulfur.<sup>61</sup> The fact that the  $\pi$ -allyl complexes with  $\text{CpCr}(\text{CO})_2$  are also known to form both exo and endo isomers—albeit non-interconverting—strengthens the bonding analogy.<sup>65</sup>

**3.6. Electrochemistry.** The cyclic voltammograms obtained of  $\text{CH}_3\text{CN}$  solutions containing **3a–e** at two different temperatures at Pt and GC electrodes are displayed in Figure 5, with all compounds giving rise to an oxidation and reduction process. On Pt, the reduction process appeared very drawn out, with an extremely wide separation between the forward and reverse peaks ( $\sim 1$  V). On GC, the reduction process appeared chemically reversible, although the anodic ( $E_p^{\text{ox}}$ ) to cathodic ( $E_p^{\text{red}}$ ) peak-to-peak separations  $\Delta E_{\text{pp}}$  were slightly wider than expected for a one-electron process (Table 4). Therefore, it is likely that the reduction process is affected by a slow rate of heterogeneous electron transfer, which is particularly slow on Pt.

The oxidation processes were complicated on both Pt and GC electrodes (Figure 5). On Pt, the  $E_p^{\text{ox}}$  peaks were particularly steep and the reverse current–potential traces often overlapped with the forward current–potential traces, especially at low temperature. Such behavior is typical of compounds that undergo adsorption during the electron-transfer process. On GC, the same voltammetric features

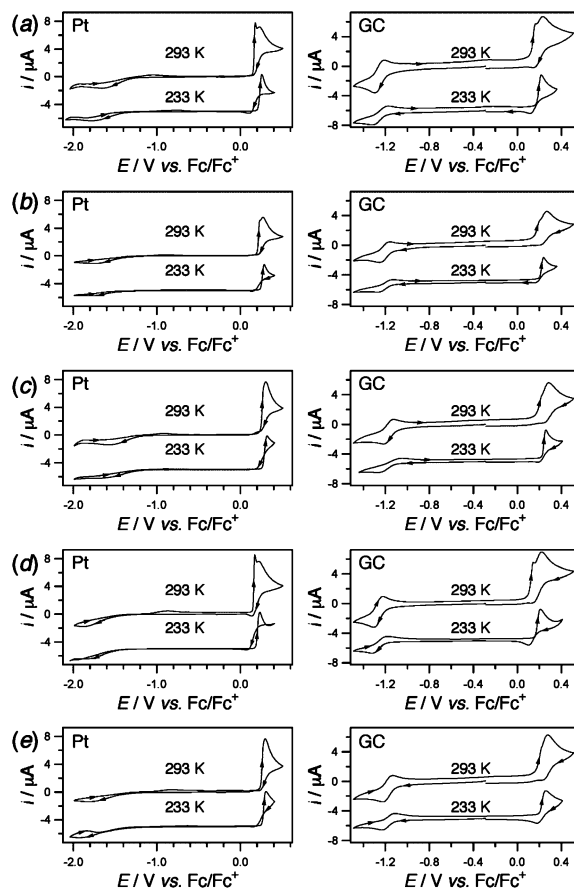


**Figure 5.** Cyclic voltammograms recorded at  $100 \text{ mV s}^{-1}$  at 1 mm planar Pt or GC electrodes in  $\text{CH}_3\text{CN}$  with  $0.25 \text{ M } ^n\text{Bu}_4\text{NPF}_6$  of 1 mM solutions of (a) **3a**, (b) **3b**, (c) **3c**, (d) **3d**, and (e) **3e**. Voltammograms at 233 K are offset by  $-5 \mu\text{A}$ .

(steep  $E_p^{\text{ox}}$  peak and overlapping current–potential traces) were evident but to a lesser extent than on Pt, suggesting less adsorption. The anodic peak current ( $i_p^{\text{ox}}$ ) for the oxidative process was much greater than the cathodic peak current ( $i_p^{\text{red}}$ ) for the reduction process, suggesting that more electrons were transferred during the oxidation, although peak currents are not necessarily indicative of the relative number of electrons transferred in processes that involve adsorption. It is likely that the reduction processes (on GC) involve the chemically reversible transfer of one-electron while the oxidative processes involves the transfer of greater than one electron. The chemical reversibility of the oxidation processes appeared to improve on GC as the temperature was lowered, especially for compounds **3a**, **3d**, and **3e**, in the sense that the  $i_p^{\text{red}}/i_p^{\text{ox}}$  ratio became closer to unity at lower temperatures.

**3.7. SEPR.** Depending on sample history, solutions of **3a–e** in  $\text{CH}_3\text{CN}/0.1 \text{ M } ^n\text{Bu}_4\text{NPF}_6$  displayed either a flat baseline or small EPR signals (a five-line pattern with  $a_{\text{N}} = 0.51 \text{ mT}$ ,  $g = 2.010$ , and a single-line pattern with  $g = 1.981$ , line width (LW) =  $0.3 \text{ mT}$ ,  $a_{\text{Cr}} = 0.85 \text{ mT}$ ), consistent with minor dissociation into free **2A**<sup>59</sup> and a Cr-centered radical, though the  $g$  value of the latter is quite different from that expected for  $\text{CpCr}(\text{CO})_2\text{NCCH}_3$ , the solvate which might reasonably result from a simple dissociation of the complex into two free radicals. (For example,  $g$  for  $\text{CpCr}(\text{CO})_2\text{NCPH}$

(65) Norman, D. W.; Ferguson, M. J.; Stryker, J. M. *Organometallics* **2004**, *23*, 2015–2019.

**Table 4.** Cyclic Voltammetric <sup>a</sup> and EPR Data

compd	reduction processes				EPR data from one-electron-reduced compounds (anion radicals) 3 <sup>•-</sup>			
	$E_p^{\text{red}}/\text{V}^b$	$E_p^{\text{ox}}/\text{V}^c$	$E_{1/2}^r/\text{V}^d$	$\Delta E/\text{mV}^e$	$g^f$	$a_N/\text{mT}^g$	LW/mT <sup>h</sup>	$t_{1/2}/\text{s}$
<b>3a</b>	-1.296	-1.212	-1.25	84	2.0085	0.597	0.072	5.7
<b>3b</b>	-1.252	-1.160	-1.21	92	2.0086	0.591	0.071	4.1
<b>3c</b>	-1.218	-1.124	-1.17	94	2.0085	0.597 <sup>i</sup>	0.069	5.6
<b>3d</b>	-1.226	-1.134	-1.18	92	2.0088	0.589 <sup>j</sup>	0.073	5.7
<b>3e</b>	-1.306	-1.222	-1.26	84	2.0088	0.587	0.072	4.0

<sup>a</sup> Obtained at a scan rate of 100 mV s<sup>-1</sup> at a 1 mm diameter GC electrode at 293 K in CH<sub>3</sub>CN with 0.25 M Bu<sub>4</sub>NPF<sub>6</sub> as the supporting electrolyte; all potentials are relative to the ferrocene/ferrocenium redox couple. <sup>b</sup>  $E_p^{\text{red}}$  = reductive peak potential. <sup>c</sup>  $E_p^{\text{ox}}$  = oxidative peak potential. <sup>d</sup>  $E_{1/2}^r = (E_p^{\text{red}} + E_p^{\text{ox}})/2$  (measured to nearest 10 mV). <sup>e</sup>  $\Delta E = |E_p^{\text{ox}} - E_p^{\text{red}}|$ . <sup>f</sup> Measured against solid dpph;  $2.0037 \pm 0.0002$ . <sup>g</sup> At 291 K in CH<sub>3</sub>CN containing 0.1 M Bu<sub>4</sub>NPF<sub>6</sub> unless otherwise noted;  $a_N$  values were found to be independent of temperature over the range 233–291 K for all 3<sup>•-</sup>. <sup>h</sup> Peak-to-peak line width in dispersion mode obtained from digital simulation in WinSim 2002,<sup>45</sup> and independent of  $T$  over the range 233–291 K for all 3<sup>•-</sup>. <sup>i</sup> At 253 K in CH<sub>3</sub>CN containing 0.1 M Bu<sub>4</sub>NPF<sub>6</sub>. <sup>j</sup> At 270 K in CH<sub>3</sub>CN containing 0.1 M Bu<sub>4</sub>NPF<sub>6</sub>.

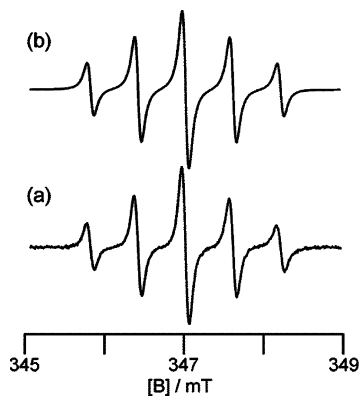


**Figure 6.** Experimental (a) and simulated (b) (WinSim 2002) EPR spectrum obtained upon the in situ electrolysis at 291 K of (8.1 mM) **3a** in CH<sub>3</sub>CN/Bu<sub>4</sub>NPF<sub>6</sub> (0.1 M) solution at a potential of -1.30 V vs Fc. The simulation employed Lorentzian line shapes with a LW of 0.072 mT,  $a_N = 0.597$  mT, and  $g = 2.0085$  measured against solid external dpph.

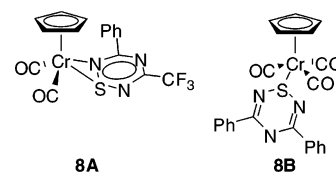
is reported to be 2.025;<sup>66</sup> the  $g$  we observe is more typical of a Cr<sup>+3</sup> species.<sup>67</sup> Upon electrolysis at the peak potentials corresponding to the oxidation processes, no new EPR signals were obtained. This is consistent with the CV evidence for greater than one electron transfer, leading either to diamagnetic products via chemical steps following the heterogeneous electron transfers or to instant adsorption onto the electrode surface. However, upon electrolysis at the cathodic peak potentials for the reduction processes listed in Table 4, a strong new five-line pattern rapidly evolves (Figure 6) that overwhelms any minor impurity signals present. The spectra of all five radicals are very similar with narrow spectral lines and hyperfine splitting constants (hfsc) of 0.587–0.597 mT to two equivalent  $I = 1$  nuclei, i.e., two <sup>14</sup>N (Table 4). There is no evidence for hyperfine coupling to <sup>53</sup>Cr ( $I = 3/2$ , 9.5% abund), as satellites of 4.75% intensity even with small  $a_{\text{Cr}}$  values should easily be observable about the sharp main spectral lines. Against the notion that the EPR spectra belong to free **2A** are the ~0.1 mT larger hfsc (all these dithiadiazolyl radicals have hfsc of 0.51 mT to two equivalent <sup>14</sup>N nuclei)<sup>59,34b</sup> and the short half-lives (4–6 s; see Table 4), whereas dithiadiazolyls are stable radicals in absence of O<sub>2</sub>.

(66) Morton, J. R.; Preston, K. F.; Cooley, N. A.; Baird, M. C.; Krusic, P. J.; McLain, S. J. *J. Chem. Soc., Faraday Trans.* **1987**, *83*, 3535–3540.

(67) (a) Atsarkin, V. A.; Gerasimova, É. A.; Matveeva, I. G.; Frantsson, A. V. *Sov. Phys. JEPT* **1963**, *16*, 903. (b) Henderson, B.; Wertz, J. E. *Defects in the Alkaline Earth Oxides*; Halstead-Wiley, New York, 1977; p 37.

These spectra are thus fully consistent with *ligand-centered* reduction of complexes **3a–e** resulting in complexed radical anions **3a–e**<sup>•-</sup> that are stabilized by CH<sub>3</sub>CN solvent, but which decay either by dissociation into **1A** and **2A**<sup>-</sup> or **1A**<sup>-</sup> and **2A**, or else by adsorption to the cell walls or onto the gold electrodes. Consistent with this, samples that had undergone repeated electrolyses showed after the decay of the signals from 3<sup>•-</sup> significantly more intense, persistent signals ( $g = 2.010$ ) attributable to **2A** as well as overlapping signals of varying LW at  $g = 2.002$ – $2.003$  with the appearance of axial powder patterns with small  $g$  anisotropies (~0.006). We attribute these latter species to radicals adsorbed on surfaces; whether they are organic or Cr-containing cannot be ascertained.

The  $a_N$  values of **3a–e**<sup>•-</sup> are independent of temperature over the range 233–291 K. A subtle trend in the size of the hfsc can be observed from 0.587 for the most electron-withdrawing aryl substituent to 0.597 mT for the donating OMe group. Curiously, no such trend is seen in the  $E_{1/2}^r$  values. These  $a_N$  values suggest that spin density within the S<sub>2</sub>N<sub>2</sub>C ring is polarized toward the nitrogen atoms (and away from sulfur) compared to **2A**. The spectral lines are much narrower than those of dithiadiazolyls at 291 K, and do not show the temperature dependence of the LW displayed by the latter.<sup>34b</sup> The line shapes are fully Lorentzian, indicating the absence of unresolved hyperfine coupling, e.g., to aryl ring <sup>1</sup>H nuclei. However, the absence of <sup>53</sup>Cr hfsc augurs against a structure for the anions directly analogous to that of the neutral complexes **3** (based on results from DFT calculations on the anion at the neutral-complex geometry). A possible insight into this conundrum is provided by our recent discovery of two distinct side-on  $\pi$ -bonding modes for the complexes between **1A** and two 7 $\pi$ -electron 1,2,4,6-thiatriazinyls (hence closely related to **2**):  $\eta^2$  (three-electron donating) in **8A** and  $\eta^1$  (one-electron donating) in **8B**.<sup>56</sup>



It is therefore possible that, upon reduction, the dithiadiazolyl ligands are partly displaced to a more weakly bonded  $\eta^1$  coordination mode, with CH<sub>3</sub>CN taking the fifth ligand

position occupied by the third CO in **8B**. We are inclined to this view, despite the apparently symmetric spectra (equivalent  $^{14}\text{N}$  nuclei). The bonding may be fluxional between the two S atoms in the solution phase, or a minor asymmetry in hfsc may be too small to resolve given the rather large spectral linewidths. What we have not yet established is whether this specific solvation by  $\text{CH}_3\text{CN}$  precedes, or follows, the one-electron reduction process.

#### 4. Conclusions

The interaction between  $[\text{CpCr}(\text{CO})_3]_2$  and dithiadiazolyl dimers  $[\text{S}_2\text{N}_2\text{CNR}]_2$  (R = substituted aryl rings) has resulted in the isolation of a series of the first  $\pi$  organometallic complexes of C,N,S-heterocyclic compounds. X-ray diffraction analyses revealed that these heterocyclic ligands are  $\eta^2$ -S,S'-bonded to the Cr center and are oriented either endo or exo with respect to the Cp ring. Thorough chemical studies demonstrate that formation of **3a–e** competes with their destruction by as yet unreacted **1**, leading to complex reaction mixtures. A dynamic NMR study of the complex with R = 4- $\text{CF}_3\text{C}_6\text{H}_4$  identified a likely intramolecular exchange process with an appreciable  $\Delta G_{298}^\ddagger$  of  $59 \pm 4 \text{ kJ mol}^{-1}$  as well as a minor dissociative process that remains in fast exchange over the temperature range 200–300 K. The measured enthalpies and equilibrium populations are in accord with data from gas-phase DFT calculations that indicate that the two isomers are very similar in energy, with the endo being  $3 \pm 1 \text{ kJ mol}^{-1}$  more stable. Cyclic voltammetry experiments indicated that **3a–e** could be reduced in a one-electron process and oxidized in a multi-electron process. However, the appearance of the oxidation/reduction processes is strongly influenced by the electrode surface (Pt or GC). On Pt, the reduction processes were affected by slow rates of heterogeneous electron transfer,

while the oxidation processes showed evidence of adsorption. In situ electrochemical-EPR spectroscopy experiments performed during the one-electron reduction of **3a–e** led to the detection of semistable anion radicals, whose half-lives were estimated by measuring the decrease in EPR signal intensities over time (average  $t_{1/2} \sim 6 \text{ s}$  at 291 K). These results speak to a versatile and largely unexplored coordination chemistry of unsaturated C–N–S heterocyclic free radicals with paramagnetic organometallic species. Further investigations of this kind are underway in our laboratories.

**Acknowledgment.** Support from the Natural Sciences and Engineering Research Council and the Alberta Ingenuity Fund of Canada, the National University of Singapore for Academic Research Grant no. R143-000-209-112 (L.Y.G.) and postgraduate scholarships (V.W.L.N., S.L.K., and T.L.R.), and the Nanyang Technological University (R.D.W. and L.Y.G.) is gratefully acknowledged. The authors also thank L. L. Koh and G. K. Tan for X-ray diffraction analyses and R. P. A. Bettens and Y. Fan for preliminary calculations performed using B3LYP/LANL2DZ.

**Supporting Information Available:** X-ray crystallographic files in CIF format of **3a–e** and **2d**; Figures S1–8, showing the temperature dependence of the  $^1\text{H}$  NMR spectra of **3d** between 200 and 300 K, detailed DNMR line fits at all measured temperatures for **3d** for the aromatic region and for the Cp region, plots of  $\ln K$  vs  $1/T$ , Eyring plots for the exchange rate study of **3d** from the Cp spectral region, atom labels and full geometric details for the optimized exo and endo isomers from DFT calculations, enlarged CV's from Figure 5, and diagrams showing the four dimers of **2d** and the unit cell packing; and Tables S1–S3, summarizing equilibrium constants from the DNMR study of **3d**, rate data from the DNMR study on **3d**, and DNMR results. This material is available free of charge via the Internet at <http://pubs.acs.org>.

IC702128F